

Optomechanical analog of two-color electromagnetically-induced transparency: Photon transmission through an optomechanical device with a two-level system

Hui Wang,^{1,2} Xiu Gu,¹ Yu-xi Liu,^{1,3,2,*} Adam Miranowicz,^{4,2} and Franco Nori^{2,5}

¹*Institute of Microelectronics, Tsinghua University, Beijing 100084, China*

²*CEMS, RIKEN, Saitama 351-0198, Japan*

³*Tsinghua National Laboratory for Information Science and Technology (TNList), Beijing 100084, China*

⁴*Faculty of Physics, Adam Mickiewicz University, 61-614 Poznań, Poland*

⁵*Physics Department, The University of Michigan, Ann Arbor, Michigan 48109-1040, USA*

(Dated: December 3, 2024)

Some optomechanical systems can be transparent to a probe field when a strong driving field is applied. These systems can provide an optomechanical analogue of electromagnetically-induced transparency (EIT). We study the transmission of a probe field through a hybrid optomechanical system consisting of a cavity and a mechanical resonator with a two-level system (qubit). The qubit might be an intrinsic defect inside the mechanical resonator, a superconducting artificial atom, or another two-level system. The mechanical resonator is coupled to the cavity field via radiation pressure and to the qubit via the Jaynes-Cummings interaction. We find that the dressed two-level system and mechanical phonon can form two sets of three-level systems. Thus, there are two transparency windows in the discussed system. We interpret this effect as an optomechanical analog of two-color EIT (or double-EIT). We demonstrate how to switch between one and two EIT windows by changing the transition frequency of the qubit. We show that the absorption and dispersion of the system are mainly affected by the qubit-phonon coupling strength and the transition frequency of the qubit.

PACS numbers: 42.50.Pq, 07.10.Cm, 37.30.+i

I. INTRODUCTION

Micro- and nano-scale mechanical resonators [1, 2] provide a platform to explore the transition from the world of quantum physics to the classical world. Such transition can be demonstrated by coupling mechanical resonators to other quantum objects [3], including superconducting qubit circuits [4–12], transmission line resonators [13–17], optical cavities [18–21], nitrogen-vacancy (NV) centers [22–24], and two-level defects [25, 26]. For example, the quantization of mechanical oscillations can be demonstrated by phonon blockade [10], which can be measured by a cavity field [27]. Experiments [28–31] showed that mechanical resonators can operate in the quantum regime. This makes it possible to couple different degrees of freedom in hybrid quantum devices [3] by using mechanical resonators as quantum transducers [32, 33], switches, or data buses [34]. Optomechanical systems can be formed [18–21] when mechanical resonators are coupled to electromagnetic fields through radiation pressure. In most recent experiments, the electromagnetic fields of the optomechanical coupling are from microwave to optical wavelengths.

It has been shown [35–40] that mechanical resonators can be used to convert optical quantum states to microwave ones via optomechanical interactions between a mechanical resonator and a single-mode field of both optical and microwave wavelengths. Hybrid electro-optomechanical systems can exhibit controllable strong Kerr nonlinearities even in the weak-coupling regime [41]. This Kerr nonlinearity can enable, in particular, the appearance of the photon blockade or the gen-

eration of nonclassical states of microwave radiation (e.g., Schrödinger cat [42] and kitten [43] states). Also when a weak coherent probe field is applied to a cavity with an optomechanical system, the mechanical resonator can act as a switch to control the probe photon transmission such that photons can pass through the cavity one by one [44–47] or two by two [48, 49] in the limit of the strong single-photon optomechanical coupling [50–53]. This phonon-induced photon blockade can be used to engineer nonclassical phonon states [54, 55] of macroscopic mechanical resonators in low frequencies. Moreover, optomechanical systems can also become transparent to a weak probe field when a strong driving field is applied to the cavity field. This is an optomechanical analogue of electromagnetically-induced transparency (EIT) [56–59].

Both a cavity field and a mechanical resonator can be coupled to other systems, thus optomechanical systems can also be important ingredients in quantum networks. We found [60] that when a two-level atomic ensemble is coupled to the cavity field of an optomechanical system, then it can be used to enhance the photon-phonon coupling through radiation pressure. We also showed [61] that EIT in a three-level atomic ensemble, interacting with a cavity field of an optomechanical system, can be significantly changed by an oscillating mirror. Optomechanical systems can also be formed by a cavity field and trapped atoms [62, 63]. It has been shown that an optomechanical analogue of EIT can be controlled by a tunable superconducting qubit [64] or a two-level atom [65, 66] coupled to a cavity. Mechanical resonators of optomechanical systems can also be coupled to their intrinsic two-level defects [67] or artificial two-level systems, e.g., two-level superconducting qubits [28]. It is known that the optomechanical EIT [56–58] can occur in bare optomechanical systems. Moreover, EIT and related Autler-Townes splitting phenom-

*Electronic address: yuxiliu@mail.tsinghua.edu.cn

ena have also been studied in superconducting artificial atomic systems (e.g., Refs. [68–70] and the many references therein). Therefore, it is an interesting question how a two-level system coupled to a mechanical resonator affects the photon transmission through optomechanical systems.

Here we study a hybrid system, consisting of an optomechanical device and a two-level system, or a two-level defect, which is coupled to a mechanical resonator described by the Jaynes-Cummings Hamiltonian. Our numerical calculations are mainly focused on resonant interactions between the low-frequency mechanical resonator and the two-level system. The latter might be an intrinsic defect inside the mechanical resonator, a superconducting artificial atom, or another two-level system. For simplicity, hereafter we just use a qubit or a two-level system to denote those kinds of systems.

A main result of our work is the observation of the optomechanical analog of two-color EIT and the demonstration how this EIT can be switched to the standard single-color EIT. We are not aware of any other works on this effect in optomechanical systems. Nevertheless, two-color EIT (or double EIT) has already been discussed in some other systems [71], e.g., in an ensemble of two-level atoms coupled to a probe light or, equivalently, a system of two-mode polaritons coupled to one transition of the Λ -type three-level atoms [72]. This effect is also closely related to the EIT in a double- Λ system. Applications of two-color EIT include nonlinear wave-mixing, cross-phase modulation, optical switching, wavelength conversion, etc.

The paper is organized as follows: In Sec. II, we describe a theoretical model and the equations of motion for the system operators. In Sec. III, we obtain steady-state solutions of the system operators and further study the stability of the system. In Sec. IV, the light transmission in this hybrid system is studied through the input-output theory. In particular, the optomechanical analogues of EIT are discussed here. We finally summarize our results in Sec. V.

II. THEORETICAL MODEL

A. Hamiltonian

As schematically shown in Fig. 1, we study a hybrid device in which a qubit is coupled to the mechanical resonator of an optomechanical device [67]. Figure 1 can also describe a system, in which a single-mode cavity field is coupled to a mechanical resonator which interacts with a two-level system as in Refs. [5, 28]. We assume that the coupling between the mechanical resonator and the two-level system is described by the Jaynes-Cummings Hamiltonian. However, the interaction between the mechanical resonator and the cavity field is described by the radiation-pressure Hamiltonian. There is no direct interaction between the two-level system and the cavity field. Thus, the Hamiltonian of the whole system can be

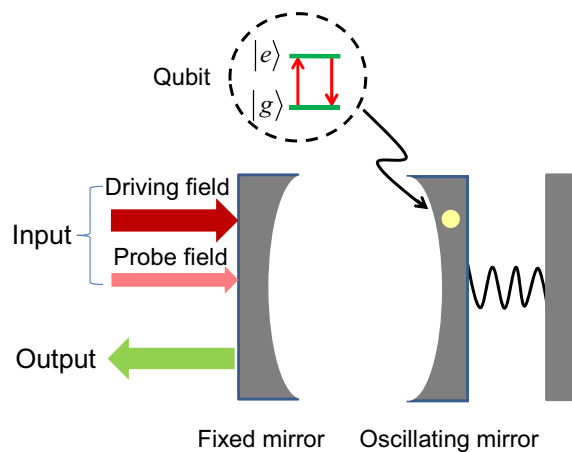


FIG. 1: (Color online) Schematic diagram of a hybrid optomechanical system consisting of a cavity (with a photonic mode a), where one of the mirrors is oscillating corresponding to a quantum mechanical resonator (with a phononic mode b). The oscillating mirror has a qubit or two-level defect denoted by two lines with the ground $|g\rangle$ and excited $|e\rangle$ states inside the dashed circle. The mechanical resonator is coupled both to the cavity (via radiation pressure) and to the qubit (via the Jaynes-Cummings interaction). However, for simplicity, we assume that there is no direct coupling between the cavity and qubit.

written as

$$H_0 = \hbar\omega_a a^\dagger a + \hbar\omega_b b^\dagger b + \frac{\hbar}{2}\omega_q \sigma_z - \hbar\chi a^\dagger a (b^\dagger + b) + \hbar g (b^\dagger \sigma_- + \sigma_+ b), \quad (1)$$

where a (a^\dagger) is the annihilation (creation) operator of the single-mode cavity field with frequency ω_a ; b (b^\dagger) is the annihilation (creation) operator of the mechanical mode with frequency ω_b . The Pauli operator σ_z is used to describe the two-level system the transition frequency ω_q , while σ_+ and σ_- are the ladder operators of the two-level system. The parameter χ is the coupling strength between the mechanical resonator and the cavity field, while the parameter g is the coupling strength between the mechanical resonator and the two-level system.

To demonstrate the relation between the cavity field and the two-level system, let us apply a unitary transform $U = \exp[-\chi a^\dagger a (b^\dagger - b)/\omega_b]$ to the Hamiltonian in Eq. (1). In this case, we have an effective Hamiltonian $H'_0 = U H_0 U^\dagger$ with

$$H'_0 = \hbar \left(\omega_a - \frac{\chi^2}{\omega_b} + \frac{g\chi}{\omega_b} \sigma_x \right) a^\dagger a - \hbar \frac{\chi^2}{\omega_b} a^\dagger a^\dagger a a + \frac{\hbar}{2}\omega_q \sigma_z + \hbar\omega_b b^\dagger b + \hbar g (b^\dagger \sigma_- + \sigma_+ b), \quad (2)$$

which shows that both the two-level system and the mechanical resonator can induce a nonlinearity in the cavity field.

Let us now assume that a strong driving field and a weak probe field, with frequencies ω_d and ω_p , respectively, are applied to the cavity. Then the Hamiltonian of the driven hybrid

system can be written as

$$H = H_0 + i\hbar (\Omega e^{-i\omega_d t} a^\dagger - \Omega^* e^{i\omega_d t} a) + i\hbar (\varepsilon e^{-i\omega_p t} a^\dagger - \varepsilon^* e^{i\omega_p t} a), \quad (3)$$

where the parameters Ω and ε , with $|\Omega| \gg |\varepsilon|$, correspond to the Rabi frequencies of the driving (i.e., pump) and probe fields, respectively. In the rotating reference frame with frequency ω_d , the Hamiltonian in Eq. (3) becomes

$$H_r = H_0 - \hbar\omega_d a^\dagger a + i\hbar (\Omega a^\dagger - \Omega^* a) + i\hbar (\varepsilon e^{-i\Delta t} a^\dagger - \varepsilon^* e^{i\Delta t} a), \quad (4)$$

with the detuning $\Delta = \omega_p - \omega_d$ between the probe field with frequency ω_p and the strong driving field with frequency ω_d .

B. Heisenberg-Langevin equations

Introducing the dissipation and fluctuation terms, and also using the Markov approximation, the Heisenberg-Langevin equations of motion can be written as

$$\dot{a} = -(\gamma_a + i\Delta_a)a + \Omega + \varepsilon \exp(-i\Delta t) + i\chi a (b^\dagger + b) + \sqrt{2\gamma_a} a_{\text{in}}(t), \quad (5)$$

$$\dot{b} = -(\gamma_b + i\omega_b)b + i\chi a^\dagger a - ig\sigma_- + \sqrt{2\gamma_b} b_{\text{in}}(t), \quad (6)$$

$$\dot{\sigma}_- = -\left(\frac{\gamma_q}{2} + i\omega_q\right)\sigma_- + igb\sigma_z + \sqrt{\gamma_q}\Gamma_-(t), \quad (7)$$

$$\dot{\sigma}_z = -\gamma_q(\sigma_z + 1) - 2ig(b\sigma_+ - b^\dagger\sigma_-) + \sqrt{\gamma_q}\Gamma_z(t). \quad (8)$$

Here γ_a , γ_b , and γ_q are the decay rates of the cavity field, mechanical mode, and two-level system, respectively. The parameter $\Delta_a = \omega_a - \omega_d$ describes the detuning between the cavity field a with frequency ω_a and the strong driving field with frequency ω_d . The operators $a_{\text{in}}(t)$, $b_{\text{in}}(t)$, $\Gamma_-(t)$, and $\Gamma_z(t)$ denote environmental noises corresponding to the operators a , b , σ_- , and σ_z . We assume that the mean values of the above noise operators are zero, that is,

$$\langle a_{\text{in}}(t) \rangle = \langle b_{\text{in}}(t) \rangle = \langle \Gamma_-(t) \rangle = \langle \Gamma_z(t) \rangle = 0. \quad (9)$$

However, their correlation functions satisfy the relations

$$\langle a_{\text{in}}^\dagger(t') a_{\text{in}}(t) \rangle = n_a \delta(t' - t), \quad (10)$$

$$\langle b_{\text{in}}^\dagger(t') b_{\text{in}}(t) \rangle = n_b \delta(t' - t), \quad (11)$$

$$\langle \Gamma_+(t') \Gamma_-(t) \rangle = n_r \delta(t' - t), \quad (12)$$

$$\langle \Gamma_+(t') \Gamma_z(t) \rangle = -2n_r \langle \sigma_+ \rangle \delta(t' - t), \quad (13)$$

$$\langle \Gamma_-(t') \Gamma_z(t) \rangle = 2(n_r + 1) \langle \sigma_- \rangle \delta(t' - t), \quad (14)$$

$$\langle \Gamma_z(t') \Gamma_z(t) \rangle = 2(2n_r + 1 + \langle \sigma_z \rangle) \delta(t' - t). \quad (15)$$

Here n_a and n_b are the mean photon and phonon numbers in thermal equilibrium, respectively; n_r is the mean number of reservoir oscillators (photons or phonons), in thermal equilibrium, interacting with the two-level system.

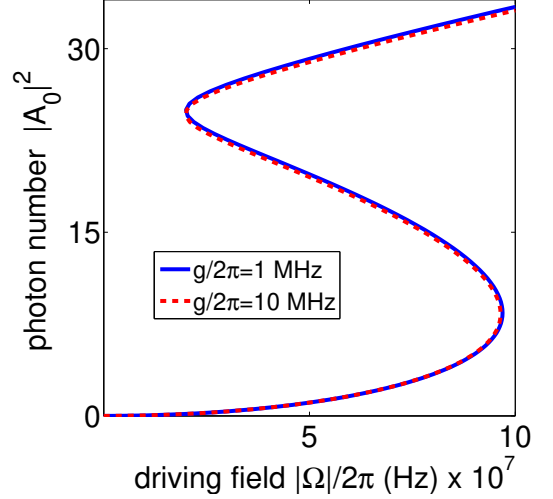


FIG. 2: (Color online) The steady-state photon number $|A_0|^2$ of the cavity field is plotted as a function of the driving field strength $|\Omega|/(2\pi)$, assuming $Z_0 = -0.99$, $g/(2\pi) = 10$ MHz, $\gamma_a/(2\pi) = 4$ MHz, $\omega_q/(2\pi) = \omega_b/(2\pi) = 100$ MHz, $\gamma_q/(2\pi) = 0.1$ MHz, $\gamma_b/(2\pi) = 1000$ Hz, $\Delta_a/(2\pi) = 50$ MHz, and $\chi/(2\pi) = 10$ MHz. Note that the frequency $\omega_b/(2\pi)$ of the mechanical mode is set to 100 MHz in the numerical calculations shown in all figures.

III. STEADY STATES AND STABILITY ANALYSIS

A. Steady states and linear response to probe field

To analyze the response of the system, in a steady state, to the weak probe field, we now take the mean values corresponding to Eqs. (5)–(8). In this case, we have the following equations

$$\langle \dot{a} \rangle = -(\gamma_a + i\Delta_a)\langle a \rangle + i\chi\langle a \rangle (\langle b^\dagger \rangle + \langle b \rangle) + \Omega + \varepsilon \exp(-i\Delta t), \quad (16)$$

$$\langle \dot{b} \rangle = -(\gamma_b + i\omega_b)\langle b \rangle + i\chi\langle a^\dagger \rangle \langle a \rangle - ig\langle \sigma_- \rangle, \quad (17)$$

$$\langle \dot{\sigma}_- \rangle = -\left(\frac{\gamma_q}{2} + i\omega_q\right)\langle \sigma_- \rangle + ig\langle b \rangle \langle \sigma_z \rangle, \quad (18)$$

$$\langle \dot{\sigma}_z \rangle = -\gamma_q(\langle \sigma_z \rangle + 1) - 2ig(\langle b \rangle \langle \sigma_+ \rangle - \langle b^\dagger \rangle \langle \sigma_- \rangle). \quad (19)$$

Here we note that the mean-field approximation, i.e., $\langle a^\dagger a \rangle = \langle a^\dagger \rangle \langle a \rangle$, was used in the derivation of these equations.

It is very unlikely to obtain exact analytical solutions of the nonlinear Eqs. (16)–(19), because the steady-state response contains an infinite number of components of different frequencies of the nonlinear systems. Instead, we find a steady-state solution, which is exact for the driving field in the parameter Ω and correct to first order in the parameter ε of the probe field. That is, we assume that the solutions of Eqs. (16)–(19) have the following forms [73]:

$$\langle a \rangle = A_0 + A_+ \exp(i\Delta t) + A_- \exp(-i\Delta t), \quad (20)$$

$$\langle b \rangle = B_0 + B_+ \exp(i\Delta t) + B_- \exp(-i\Delta t), \quad (21)$$

$$\langle \sigma_- \rangle = L_0 + L_+ \exp(i\Delta t) + L_- \exp(-i\Delta t), \quad (22)$$

$$\langle \sigma_z \rangle = Z_0 + Z_+ \exp(i\Delta t) + Z_- \exp(-i\Delta t). \quad (23)$$

Here A_0 , B_0 , L_0 , and Z_0 correspond to the solutions of a , b , σ_- , and σ_z , respectively, when only the driving field is applied. The parameters A_{\pm} , B_{\pm} , L_{\pm} , and Z_{\pm} are of the order of ε of the probe field. These can be obtained by substituting Eqs. (20)–(23) into Eqs. (16)–(19) and comparing the coefficients of the same order. For example, we substitute the expressions $\langle b \rangle$, $\langle \sigma_- \rangle$, and $\langle \sigma_z \rangle$, given by Eqs. (21)–(23), into Eq. (19), then Z_0 , Z_+ , and Z_- can be expressed in terms of L_0 , L_+ , L_- , B_0 , B_+ , and B_- as follows

$$Z_0 = 2i \frac{g}{\gamma_q} (B_0^* L_0 - B_0 L_0^*) - 1, \quad (24)$$

$$Z_+ = -\lambda_1 (B_0 L_-^* + L_0^* B_+ - B_0^* L_+ - L_0 B_-^*), \quad (25)$$

$$Z_- = \lambda_1^* (B_0 L_+^* + L_0^* B_- - B_0^* L_- - L_0 B_+^*), \quad (26)$$

with $\lambda_1 = 2g/(\Delta - i\gamma_q)$. Since σ_z is a Hermitian operator, the conditions $Z_0^* = Z_0$, $Z_+^* = Z_-$, and $Z_-^* = Z_+$ have been used when Eqs. (24)–(26) were derived. Similarly, we obtain

$$L_0 = \frac{2gB_0Z_0}{2\omega_q - i\gamma_q}. \quad (27)$$

Since the two-level system is coupled only to the mechanical mode, then the steady-state value L_0 is directly related only to the steady-state value of the mechanical mode and indirectly related to those of the cavity field. We find that L_+ and L_- can be expressed with B_+ and B_- as

$$L_+ = \lambda_2 B_+ + \lambda_3 B_-^*, \quad (28)$$

$$L_- = \lambda_4 B_- + \lambda_5 B_+^*. \quad (29)$$

Explicit formulas for these and other parameters λ_i ($i = 2, 3, \dots, 10$) are given in the Appendix .

We substitute L_0 , given by Eq. (27), into Eq. (24), and then obtain the solution

$$Z_0 = -\frac{\gamma_q^2 + 4\omega_q^2}{\gamma_q^2 + 4\omega_q^2 + 8g^2|B_0|^2}. \quad (30)$$

It is easy to find that the value of Z_0 ranges from -1 to 0 . If $Z_0 = -1$, then the two-level system is in its ground state. Thus, it is obvious that if the coupling strength g is much smaller than the transition frequency ω_q of the two-level system, and the phonon number is not very large, then the two-level system is almost in its ground state. We also obtain

$$B_0 = \frac{\chi|A_0|^2 - gL_0}{\omega_b - i\gamma_b}, \quad (31)$$

$$B_+ = \lambda_6(A_0^* A_+ + A_0 A_-^*), \quad (32)$$

$$B_- = \lambda_7(A_0^* A_- + A_0 A_+^*), \quad (33)$$

where B_0 is the steady-state value of the mechanical mode. Because of the coupling of the mechanical mode to the two-level system and the cavity field, B_0 depends both on the steady-state values L_0 of the two-level system and on the steady-state value A_0 of the cavity field.

We now calculate the coefficients of the steady-state value of the cavity field by substituting the expansions of $\langle a \rangle$, given

by Eq. (20), and $\langle b \rangle$, given by Eq. (21), into Eq. (16). Up to first order in the parameter ε , we obtain

$$A_0 = \frac{\Omega}{\gamma_a + i\Delta_a - i\chi(B_0 + B_0^*)}, \quad (34)$$

which represents the steady-state value of the cavity field assuming a strong driving field. With the help of Eqs. (32)–(34), we also obtain

$$A_- = \frac{\lambda_9 \varepsilon}{\lambda_8 \lambda_9 - \lambda_{10}}, \quad (35)$$

which describes the response of the strongly-driven system to the weak-probe field, when the driven system reaches a steady state. Similarly, we also obtain

$$A_+ = \frac{i\chi(\lambda_6 + \lambda_7) A_0^2 \varepsilon^*}{\lambda_8^* \lambda_9^* - \lambda_{10}^*}, \quad (36)$$

which describes the four-wave mixing for the driving field and the weak probe field.

B. Stability

To analyze the stability of the system, we now present the driving field strength $|\Omega|$ (i.e., the Rabi frequency of the driving field) as a function of the steady value of $|A_0|$ as follows

$$|\Omega| = |A_0| \sqrt{\gamma_a^2 + \left[\Delta_a - \frac{2\chi^2 \varepsilon_2 |A_0|^2 (\gamma_a^2 + 4\omega_q^2)}{\varepsilon_1^2 + \varepsilon_2^2} \right]^2} \quad (37)$$

with the parameters ε_1 and ε_2 given by

$$\varepsilon_1 = \gamma_b (\gamma_a^2 + 4\omega_q^2) - 2\gamma_a g^2 Z_0, \quad (38)$$

$$\varepsilon_2 = \omega_b (\gamma_a^2 + 4\omega_q^2) + 4\omega_q g^2 Z_0. \quad (39)$$

We can conclude from Eq. (30) that if the coupling strength $g \ll \omega_q$ and the phonon number are small then the two-level system has a high possibility to remain in its ground state. In this case the value of Z_0 is very close to -1 and can be considered constant, then we can see from Eq. (37) that $|A_0|$ can have three real solutions under certain conditions.

In Fig. 2, the steady-state photon number $|A_0|^2$ of the cavity field, corresponding to the steady-state component in Eq. (20), is plotted as a function of the driving field strength $|\Omega|$. This figure shows the bistable behavior of the cavity field of the hybrid optomechanical system. This result is very similar to that of driven optomechanical systems [74]. If we change the coupling strength between the phonon and the two-level system, the steady value and bistable behavior change.

The relation between the phonon mode B_0 and the Rabi frequency Ω can also be calculated as

$$|\Omega|^2 = \frac{[\gamma_a^2 + (\Delta_a - 2\chi \text{Re} B_0)^2] (\varepsilon_4 + i\varepsilon_5) B_0}{i\chi\varepsilon_3} \quad (40)$$

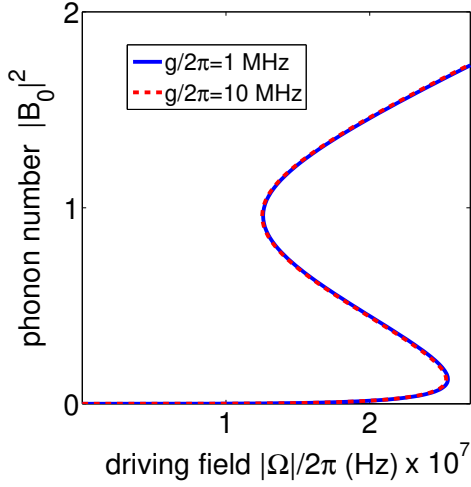


FIG. 3: (Color online) The steady-state phonon number $|B_0|^2$ of the mechanical mode is plotted as a function of the driving field strength $|\Omega|/(2\pi)$. The other parameters are the same as in Fig. 2, except that $\Delta_a/(2\pi) = 20$ MHz.

with the parameters given by

$$\varepsilon_3 = \gamma_a^2 + 4\omega_q^2 \quad (41)$$

$$\varepsilon_4 = \gamma_b \varepsilon_3 - 2\gamma_a g^2 Z_0 \quad (42)$$

$$\varepsilon_5 = \omega_b \varepsilon_3 + 4\omega_q g^2 Z_0 \quad (43)$$

In Fig. 3, the steady-state phonon number $|B_0|^2$ of the mechanical mode, corresponding to the steady-state component in Eq. (21), is plotted as a function of the Rabi frequency $|\Omega|$ of the driving field. We find that the phonon bistability can also occur for the mechanical mode in some parameter regimes, and the two-level system has a little effect on the bistability. From Eqs. (37) and (40), if the variation of Z_0 cannot be ignored, we find that both $|A_0|$ and $|B_0|$ can have at most five real solutions, so both the photon and phonon modes can show multistability under certain conditions. According to our numerical calculations shown in Figs. 2 and 3, if the coupling strength g is much smaller than ω_b (or ω_q), the photon and phonon modes only exhibit the bistable behavior, no multistability. We note that multistability can occur when the coupling between the two-level system and the phonon mode become very strong or ultrastrong. This coupling might not be easy to produce using natural qubits. However they might become possible using an artificial two-level system, e.g., when the mechanical mode is coupled to a superconducting qubit instead of an intrinsic natural two-level defect.

IV. ELECTROMAGNETICALLY-INDUCED TRANSPARENCY

We now study the transmission of a weak-probe field through an optomechanical system which is coupled to a two-

level system. Using the input-output theory [75]

$$\langle a_{\text{out}} \rangle + \frac{\Omega}{\sqrt{2\gamma_a}} + \frac{\varepsilon}{\sqrt{2\gamma_a}} e^{-i\Delta t} = \sqrt{2\gamma_a} \langle a \rangle, \quad (44)$$

the output of the cavity field can be obtained as

$$\langle a_{\text{out}} \rangle = A_d + A_s \varepsilon e^{-i\Delta t} + A_{as} \varepsilon^* e^{i\Delta t}, \quad (45)$$

with coefficients

$$A_d = \sqrt{2\gamma_a} A_0 - \frac{\Omega}{\sqrt{2\gamma_a}}, \quad (46)$$

$$A_s = \frac{\sqrt{2\gamma_a}}{\varepsilon} A_- - \frac{1}{\sqrt{2\gamma_a}}, \quad (47)$$

$$A_{as} = \frac{\sqrt{2\gamma_a}}{\varepsilon^*} A_+. \quad (48)$$

Here A_0 and A_{\pm} are given by Eqs. (34)–(36); A_d is the output responding to the driving (or control) field with frequency ω_d , A_s is the output corresponding to the probe field with frequency ω_p (Stokes frequency), and A_{as} represents the four-wave mixing frequency $2\omega_d - \omega_p$ (anti-Stokes frequency). We redefine the output field at the frequency ω_p of the probe field as $\varepsilon_T = 2\gamma_a A_- / \varepsilon$ with the real and imaginary parts $\mu_p = \gamma_a (A_- + A_-^*) / \varepsilon$ and $\nu_p = \gamma_a (A_- - A_-^*) / (i\varepsilon)$. It is clear that μ_p and ν_p describe absorption and dispersion to the probe field.

For convenience, let us assume that $\varepsilon = \sqrt{2\gamma_a P_s / \hbar \omega_p}$ is real. Here P_s is defined as the input power of the probe field. Then the output power at the Stokes frequency relative to the input power P_s is

$$G_s = \frac{\hbar \omega_p |\varepsilon A_s|^2}{P_s} = |\sqrt{2\gamma_a} A_s|^2. \quad (49)$$

The output power at the anti-Stokes frequency $2\omega_d - \omega_p$ is [76]:

$$G_{as} = \frac{\hbar(2\omega_d - \omega_p) |\varepsilon A_{as}|^2}{P_s} = |\sqrt{2\gamma_a} A_{as}|^2. \quad (50)$$

In the resolved sideband limit $\omega_b \gg \gamma_a$, it is known that the transmission spectrum exhibits an EIT analogue in optomechanical systems. These phenomena can be mapped to the Λ -type three-level diagram of atomic systems. However, when the mechanical resonator of the optomechanical system is coupled to a two-level system, the transmission of the probe field becomes complicated. This is because the Jaynes-Cummings coupling between the two-level system and the mechanical resonator can lead to dressed states, which have a more complicated energy structure.

In order to better understand the physical meaning of these results, let us use the single-photon and single-phonon excitations as an example to illustrate the nature of photon transmission in this hybrid system. The energy-level diagram for the EIT analogue in optomechanical systems can be understood as in Ref. [57]: the Λ -type three-level systems formed by three states $|0_a, 0_b\rangle$, $|0_a, 1_b\rangle$, and $|1_a, 0_b\rangle$. Here the subscripts a and

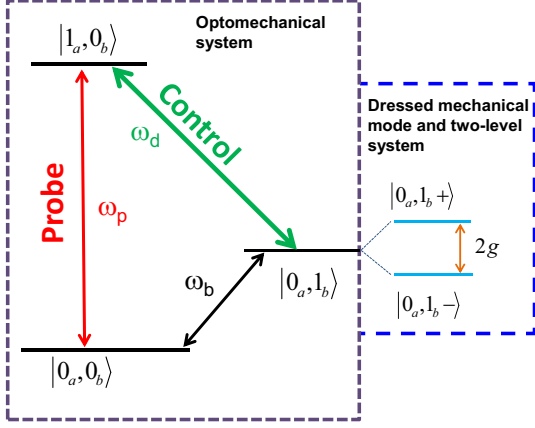


FIG. 4: (Color online) Schematic diagram for the interaction between the hybrid system with the driving (control) and probe fields with a single-particle excitation. The driving field is applied to make a single-phonon transition from the phonon vacuum state $|0_b\rangle$ to the single-phonon state $|1_b\rangle$. The probe field is used to measure the transition when the population of the mechanical mode is not changed. The Λ -type three energy levels in the hybrid optomechanical system occur in the case $\Delta_a = \omega_b$. Here $|1_b\pm\rangle = (|1_b, g\rangle \pm |0_b, e\rangle)/\sqrt{2}$ correspond to the dressed states between the single-phonon state and the two-level system for $\omega_b = \omega_q$.

b denote the photon and phonon states, respectively. However, when a two-level system is coupled to the mechanical resonator, the state $|0_a, 1_b\rangle$ is split into two states $|0_a, 1_b+\rangle$ and $|0_a, 1_b-\rangle$. Here $|1_b\pm\rangle$ denote the dressed states [77] formed by the single-phonon state and the two-level system, e.g., $|1_b\pm\rangle = (|1_b, g\rangle \pm |0_b, e\rangle)/\sqrt{2}$ for $\omega_b = \omega_q$. This splitting of the single-phonon state significantly affects the photon transmission if the detuning between the cavity field and the driving field resonant with the frequency of the mechanical resonator, i.e., $\Delta_a = \omega_b$. Clearly this splitting leads to two transparency windows, which coincide well with the numerical calculation shown in Fig. 5 and described below. The case of multi-phonon excitations is very similar to the single-phonon excitation, but the splitting width of the transparency windows becomes wider. Moreover, the nonlinear coupling between the cavity field and mechanical resonator makes the transmission spectrum more complicated when the excitation numbers of the photon and phonon are increased.

Figures 5(a) and 5(b) show, respectively, the absorption and dispersion of the probe field for different values of the coupling strength g between the mechanical resonator and the two-level system. These figures show a familiar transparency window of the optomechanical system, which can occur when there is no coupling of the two-level system to the mechanical resonator (as shown by the blue solid curves in Fig. 5). However, two transparency windows can occur when the two-level system is coupled to the mechanical resonator (as shown, e.g., by the red dashed curves in Fig. 5). The splitting of these two transparency windows is equal to the splitting width $2g$ that results from the Jaynes-Cummings coupling between the two-level system and the mechanical mode. In Fig. 6, the Stokes

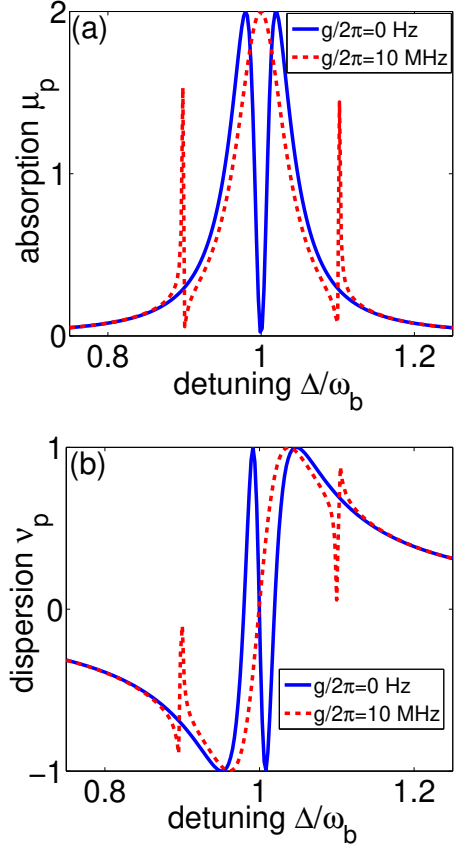


FIG. 5: (Color online) (a) Absorption μ_p and (b) dispersion ν_p versus the detuning $\Delta = \omega_p - \omega_d$ of the probe field in units of the mechanical-mode frequency ω_b . In each figure, the curves correspond to different values [0 MHz (blue solid curve) and 10 MHz (red dashed curve)] of the coupling strength $g/(2\pi)$ between the mechanical resonator and the two-level system. The other parameters are the same as in Fig. 2, except $\Delta_a/(2\pi) = 100$ MHz and $|\Omega|/(2\pi) = 19.8$ MHz. The blue and red curves describe the properties of the single (standard) and double (or two-color) optomechanical EIT effects, respectively.

and anti-Stokes power spectra are plotted as a function of the frequency of the probe field. These spectra also show that the two-level system changes the splitting width of the output spectra at the Stokes and anti-Stokes frequencies.

In addition to the coupling strength g between the two-level system and the mechanical resonator, the transition frequency ω_q of two-level system also affects the transmission of the probe field, which will even more clearly show the main result of our work, which is the finding of the optomechanical analog of two-color EIT and the demonstration of its switching to the standard single-color EIT.

In Fig. 7, the absorption spectra of the probe field are plotted as a function of the detuning Δ between the probe and driving fields. Different panels of Fig. 7 show the spectra for different values of the transition frequency of the two-level system in comparison to the mechanical-mode frequency. We observe in Fig. 7(a) that there are two nearly symmetric transparency windows [shown also by the red dashed curve in

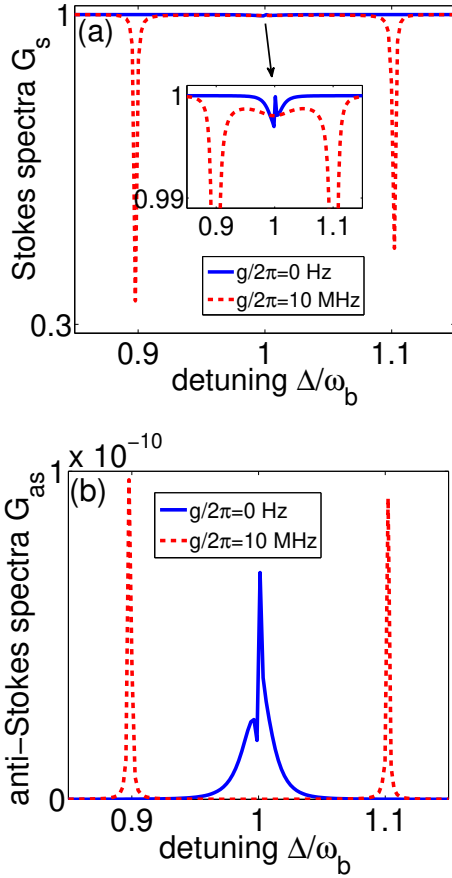


FIG. 6: (Color online) (a) The Stokes G_s and (d) anti-Stokes G_{as} spectra of the output of the probe field versus the detuning $\Delta = \omega_p - \omega_d$ of the probe field in units of the mechanical-mode frequency ω_b . The parameters are the same as in Fig. 5.

Fig. 5(a)] when the two-level system resonates with the mechanical resonator. We refer to this effect as the *optomechanical analog of two-color EIT*. However, these two transparency windows become asymmetric when the two-level system is detuned from the mechanical resonator frequency (as shown in other panels of Fig. 7). When the detuning $|\omega_q - \omega_b|$ becomes much larger than the coupling strength g , as in the cases shown in Figs. 7(d,e), these two transparency windows combine into one, almost symmetric, window, which is very similar to that of the optomechanical resonator without the qubit, as shown by the blue solid curve in Fig. 5(a). Thus, it is seen how to switch between one and two transparency windows by changing the transition frequency of the qubit, in particular how to approach the standard symmetric EIT window in the far-detuning limits for $|\omega_q - \omega_b| \gg g$. This change from two-color EIT to single-color EIT, by detuning the qubit transition frequency ω_q out of the resonance with the mechanical-mode frequency ω_b , can also be observed in other spectra. Our examples include: (i) the dispersion spectra in Fig. 8, which can be compared with Fig. 5(b); (ii) the Stokes spectra, i.e., the power spectra of the output at the Stokes frequency, as shown in Fig. 9(a) and to be compared with Fig. 6(a); and, analogously, (iii) the anti-Stokes spectra presented in Fig. 9(b).

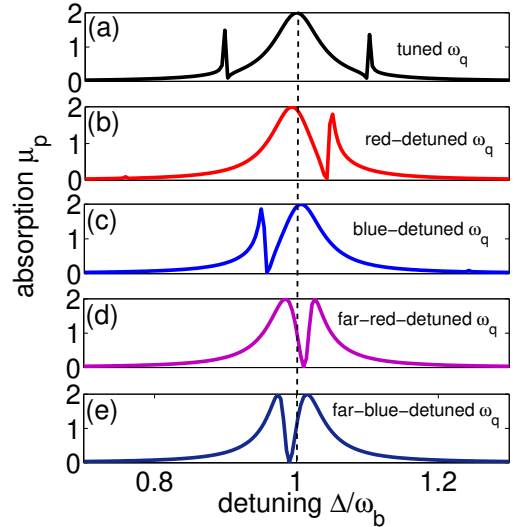


FIG. 7: (Color online) The absorption μ_p of the probe field as a function of the detuning $\Delta = \omega_p - \omega_d$ between the probe frequency ω_p and the driving field frequency ω_d for different values of the qubit transition frequency: (a) $\omega_q/(2\pi) = 100$ MHz, which corresponds to the resonance of ω_q with the mechanical-mode frequency ω_b ; (b) $\omega_q/(2\pi) = 80$ MHz (i.e., $\omega_q < \omega_b$); (c) $\omega_q/(2\pi) = 120$ MHz (i.e., $\omega_q > \omega_b$), (d) $\omega_q/(2\pi) = 10$ MHz (i.e., $\omega_b - \omega_q \gg g$), and (e) $\omega_q/(2\pi) = 200$ MHz (i.e., $\omega_q - \omega_b \gg g$). The other parameters are the same as in Fig. 2, except $\Delta_a/(2\pi) = 100$ MHz and $|\Omega|/(2\pi) = 19.8$ MHz. The absorption spectrum shown in panel (a) explains the occurrence of the optomechanical analog of two-color EIT. By contrast, the spectra in the other panels exhibit only single transparency windows. In particular, for far detunings shown in panels (d,e), the EIT windows can roughly approximate the symmetric EIT window for the standard optomechanical single-color EIT, when there is no coupling between the mechanical resonator and the qubit, as shown by the blue curve in Fig. 5(a). Thus, it is seen how to switch between the single and double transparency windows simply by tuning the qubit transition frequency in or out of the resonance with the mechanical-mode frequency.

This figure can be compared with Fig. 6(b).

V. CONCLUSIONS

In summary, we have studied the transmission of a probe field through an optomechanical system, consisting of a cavity and a mechanical resonator with a two-level system, for simplicity referred to as a qubit. The qubit might be an intrinsic defect inside the mechanical resonator, a superconducting artificial atom, or another two-level system. We assume that the mechanical resonator is coupled to the qubit via the Jaynes-Cummings interaction and to the cavity field via radiation pressure.

We find that the transmission of the probe field exhibits two transparent windows when the two-level system is resonantly coupled to the mechanical resonator. This is because the interaction between the mechanical resonator and the two-level system might result in two sets of coupling configurations be-

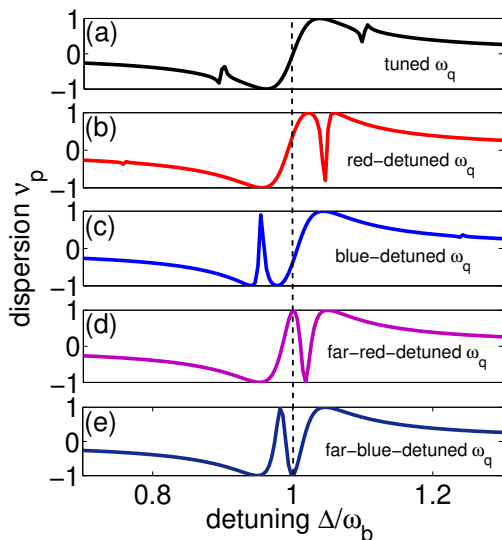


FIG. 8: (Color online) Same as in Fig. 7 but for the dispersion spectra ν_p of the probe field.

tween the controlling field and the mechanical resonator. We consider this effect as an optomechanical analog of two-color EIT (or double EIT), in contrast to the standard optomechanical single-color (or single-window) EIT exhibiting clear differences in the probe-field spectra. Our examples include: the absorption, dispersion, Stokes, and anti-Stokes spectra. We demonstrated how to switch between one and two EIT windows by changing the transition frequency of the qubit to be in or out of the resonance with the frequency of the mechanical mode. These features might be used to probe the low-frequency two-level fluctuations inside solid-state systems by using a low-frequency mechanical resonator. We note that the control of the transition frequency of the qubit could be realized easier with an artificial two-level system (e.g., a superconducting qubit) rather than with a natural two-level defect.

In addition to optical switching, applications of the optomechanical two-color EIT can include: the generation of nonclassical states of microwave radiation and/or mechanical resonator, nonlinear wave-mixing, cross-phase modulation, wavelength conversion or photon blockade [78], in analogy to such applications of the standard optomechanical single-color EIT.

We hope that our study, in particular, the finding of the optomechanical analog of two-color EIT, which can be switched to the standard single-color EIT, might provide a new method to control the light transmission through optomechanical systems by using a two-level system and to probe a low-frequency two-level system by using a mechanical resonator.

VI. ACKNOWLEDGEMENT

We thank Hui Jing and Jieqiao Liao for insightful and informative discussions. Y.X.L. is supported by the National Natural Science Foundation of China under Grant Nos. 61025022,

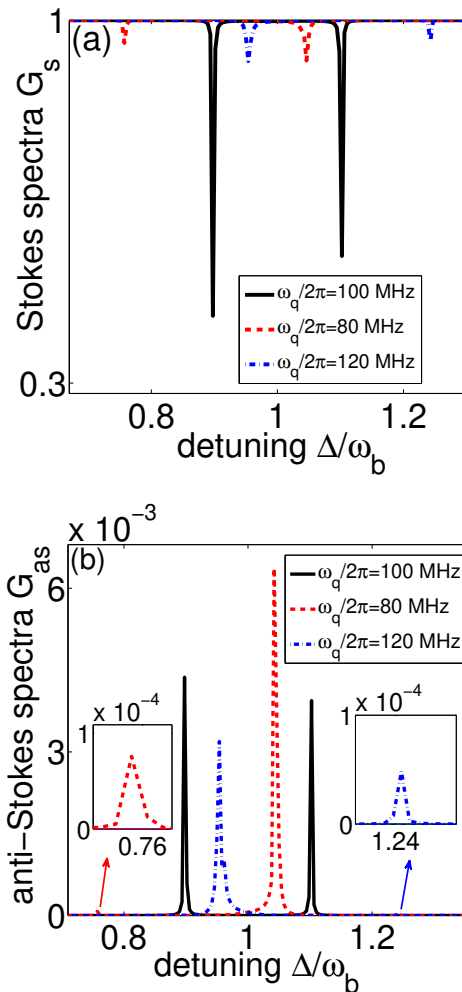


FIG. 9: (Color online) The Stokes G_s and anti-Stokes G_{as} spectra of the output of the probe field versus the detuning $\Delta = \omega_p - \omega_d$. In each figure, three curves correspond to different transition frequencies of the qubit: (i) $\omega_q/(2\pi) = 100$ MHz (black solid curve) being in resonance with the mechanical-mode frequency ω_b , as shown in Figs. 7(a) and 8(a); (ii) $\omega_q/(2\pi) = 80$ MHz (red dashed curve) corresponding to the case of the red-detuned ω_q shown in Figs. 7(b) and 8(b); and (iii) $\omega_q/(2\pi) = 120$ MHz (blue dash-dotted curve) corresponding to the case of the blue-detuned ω_q shown in Figs. 7(c) and 8(c). All the parameters are the same as in the respective Figs. 7 and 8.

61328502, the National Basic Research Program of China Grant No. 2014CB921401. A.M. is supported by Grant No. DEC-2011/03/B/ST2/01903 of the Polish National Science Centre. F.N. is partially supported by the RIKEN iTHES Project, MURI Center for Dynamic Magneto-Optics, JSPS-RFBR contract No. 12-02-92100, Grant-in-Aid for Scientific Research (S), MEXT Kakenhi on Quantum Cybernetics, and the JSPS via its FIRST program.

Appendix: Calculation of A_+ and A_-

From the discussions in Sec. III, one can find the expressions of Z_0 , Z_+ , Z_- , L_0 , L_+ , and L_- in Eqs. (24)–(29) up to first order in the parameter ε of the probe field by equating the coefficients of the same order. Then the corresponding coefficients are found to be

$$\lambda_2 = \frac{1}{D_3} [igZ_0D_1 - g\lambda_1B_0L_0^* (iD_1 - g\lambda_1|B_0|^2)], \quad (\text{A.1})$$

$$\lambda_3 = i\frac{g\lambda_1B_0}{D_3} (ig\lambda_1|B_0|^2L_0 + igB_0Z_0 + D_1L_0), \quad (\text{A.2})$$

$$\lambda_4 = \frac{1}{D_3^*} [igZ_0D_2 + g\lambda_1^*B_0L_0^* (iD_2 + g\lambda_1^*|B_0|^2)], \quad (\text{A.3})$$

$$\lambda_5 = i\frac{g\lambda_1^*B_0}{D_3^*} (ig\lambda_1^*|B_0|^2L_0 - igB_0Z_0 - D_2L_0), \quad (\text{A.4})$$

where the parameters D_1 , D_2 , and D_3 are given by

$$D_1 = \frac{\gamma_q}{2} - i\omega_q - ig\lambda_1|B_0|^2 + i\Delta, \quad (\text{A.5})$$

$$D_2 = \frac{\gamma_q}{2} - i\omega_q + ig\lambda_1^*|B_0|^2 - i\Delta, \quad (\text{A.6})$$

$$D_3 = \left(\frac{\gamma_q}{2} + i\Delta\right)^2 - 2ig\lambda_1|B_0|^2 \left(\frac{\gamma_q}{2} + i\Delta\right) + \omega_q^2. \quad (\text{A.7})$$

By substituting the expressions of $\langle b \rangle$, $\langle a \rangle$, and $\langle \sigma_- \rangle$ into the equation of motion for the average value of the operator b , we

obtain the expressions of B_0 , B_+ , and B_- in Eqs. (31)–(33). Here the coefficients λ_6 and λ_7 are found as

$$\lambda_6 = \frac{-g\chi\lambda_3 + i\chi D_4}{D_4D_5 - g^2\lambda_3\lambda_5^*}, \quad (\text{A.8})$$

$$\lambda_7 = \frac{-g\chi\lambda_5 + i\chi D_5^*}{D_4^*D_5^* - g^2\lambda_3^*\lambda_5}. \quad (\text{A.9})$$

with

$$D_4 = \gamma_b - i(\omega_b - \Delta + g\lambda_4^*), \quad (\text{A.10})$$

$$D_5 = \gamma_b + i(\omega_b + \Delta + g\lambda_2). \quad (\text{A.11})$$

Using similar steps as above, we obtain formulas for A_0 , A_- , and A_+ for the average value of the cavity field, up to first order in the parameter ε of the probe field as given, respectively, by Eqs. (34)–(36) with the parameters

$$\lambda_8 = \gamma_a + i[\Delta_a - \Delta - \chi B_0 - \chi(\lambda_6^* + \lambda_7)|A_0|^2],$$

$$\lambda_9 = \gamma_a - i[\Delta_a + \Delta - \chi B_0^* - \chi(\lambda_6^* + \lambda_7)|A_0|^2],$$

$$\lambda_{10} = \chi^2(\lambda_6^* + \lambda_7)^2|A_0|^4.$$

It is clear that A_0 represents the steady-state value of the cavity field when the probe field is not applied to the cavity. However, A_- describes the linear response of the system to the probe field, and A_+ describes the four-wave mixing of the probe and driving fields.

-
- [1] M.P. Blencowe, Phys. Rep. **395**, 159 (2004).
[2] M. Poot and H. S. J. van der Zant, Phys. Rep. **511**, 273 (2012).
[3] Z. L. Xiang, S. Ashhab, J. Q. You, and F. Nori, Rev. Mod. Phys. **85**, 623 (2013).
[4] E. K. Irish and K. Schwab, Phys. Rev. B **68**, 155311 (2003).
[5] A. D. Armour, M. P. Blencowe, and K. C. Schwab, Phys. Rev. Lett. **88**, 148301 (2002).
[6] A. T. Sornborger, A. N. Cleland, and M. R. Geller, Phys. Rev. A **70**, 052315 (2004).
[7] A. N. Cleland and M. R. Geller, Phys. Rev. Lett. **93**, 070501 (2004); M. R. Geller and A. N. Cleland, Phys. Rev. A **71**, 032311 (2005).
[8] L. Tian, Phys. Rev. B **72**, 195411 (2005).
[9] L. F. Wei, Y. X. Liu, C. P. Sun, and F. Nori, Phys. Rev. Lett. **97**, 237201 (2006).
[10] Y. X. Liu, A. Miranowicz, Y. B. Gao, J. Bajer, C. P. Sun, and F. Nori, Phys. Rev. A **82**, 032101 (2010).
[11] M. D. LaHaye, J. Suh, P. M. Echternach, K. C. Schwab, and M. L. Roukes, Nature (London) **459**, 960 (2009).
[12] F. Xue, Y. X. Liu, C. P. Sun, and F. Nori, Phys. Rev. B **76**, 064305 (2007).
[13] F. Xue, Y. D. Wang, Y. X. Liu, and F. Nori, Phys. Rev. B **76**, 205302 (2007).
[14] Y. Li, Y.-D. Wang, F. Xue, and C. Bruder, Phys. Rev. B **78**, 134301 (2008).
[15] T. Rocheleau, T. Ndikum, C. Macklin, J. B. Hertzberg, A. A. Clerk, and K. C. Schwab, Nature (London) **463**, 72 (2010).
[16] J. B. Hertzberg, T. Rocheleau, T. Ndikum, M. Savva, A. A. Clerk, and K. C. Schwab, Nat. Phys. **6**, 213 (2010).
[17] F. Massel, T. T. Heikkilä, J.-M. Pirkkalainen, S. U. Cho, H. Saloniemi, P. J. Hakonen, and M. A. Sillanpää, Nature (London) **480**, 351 (2011).
[18] T. J. Kippenberg and K. J. Vahala, Science **321**, 1172 (2008).
[19] M. Aspelmeyer, S. Gröblacher, K. Hammerer, and N. Kiesel, J. Opt. Soc. Am. B **27**, A189 (2010).
[20] M. Aspelmeyer, P. Meystre, and K. Schwab, Phys. Today **65**, 29 (2012).
[21] M. Aspelmeyer, T. J. Kippenberg, and F. Marquardt, arXiv:1303.0733.
[22] O. Arcizet, V. Jacques, A. Siria, P. Poncharal, P. Vincent, and S. Seidelin, Nat. Phys. **7**, 879 (2011).
[23] S. Kolkowitz, A. C. B. Jayich, Q. P. Unterreithmeier, S. D. Bennett, P. Rabl, J. G. E. Harris, and M.D. Lukin, Science **335**, 1603 (2012).
[24] S. D. Bennett, N. Y. Yao, J. Otterbach, P. Zoller, P. Rabl, and M. D. Lukin, Phys. Rev. Lett. **110**, 156402 (2013).
[25] L. Tian, Phys. Rev. B **84**, 035417 (2011).
[26] G. J. Grabovskij, T. Peichel, J. Lisenfeld, G. Weiss, and A. V. Ustinov, Science **338**, 232 (2012).
[27] N. Didier, S. Pugnetti, Y. M. Blanter, and R. Fazio, Phys. Rev. B **84**, 054503 (2011).
[28] A. D. O'Connell, M. Hofheinz, M. Ansmann, R. C. Bialczak, M. Lenander, E. Lucero, M. Neeley, D. Sank, H. Wang, M. Weides, J. Wenner, J. M. Martinis, and A. N. Cleland, Nature (London) **464**, 697 (2010).
[29] J. D. Teufel, T. Donner, D. Li, J. W. Harlow, M. S. Allman, K. Cicak, A. J. Sirois, J. D. Whittaker, K. W. Lehnert, and R. W. Simmonds, Nature (London) **475**, 359 (2011).

- [30] J. Chan, T. P. M. Alegre, A. H. Safavi-Naeini, J. T. Hill, A. Krause, S. Groblacher, M. Aspelmeyer, and O. Painter, *Nature (London)* **478**, 89 (2011).
- [31] E. Verhagen, S. Deleglise, S. Weis, A. Schliesser, and T. J. Kippenberg, *Nature (London)* **482**, 63 (2012).
- [32] C. P. Sun, L. F. Wei, Y. X. Liu, and F. Nori, *Phys. Rev. A* **73**, 022318 (2006).
- [33] J.-M. Pirkkalainen, S. U. Cho, J. Li, G. S. Paraoanu, P. J. Hakonen, and M. A. Sillanpää, *Nature (London)* **494**, 211(2013).
- [34] M. Gao, Y. X. Liu, and X. B. Wang, *Phys. Rev. A* **83**, 022309 (2011).
- [35] L. Tian and H. Wang, *Phys. Rev. A* **82**, 053806 (2010).
- [36] Y. D. Wang and A. A. Clerk, *Phys. Rev. Lett.* **108**, 153603 (2012).
- [37] L. Tian, *Phys. Rev. Lett.* **108**, 153604 (2012).
- [38] J. T. Hill, A. H. Safavi-Naeini, J. Chan, and O. Painter, *Nat. Commun.* **3**, 1196 (2012).
- [39] C. H. Dong, V. Fiore, M. C. Kuzyk, and H. Wang, *Science* **338**, 1609 (2012).
- [40] J. Bochmann, A. Vainsencher, D. Awschalom, and A. N. Cleland, *Nat. Phys.* **9**, 712 (2013).
- [41] X.Y. Lü, W.M. Zhang, S. Ashhab, Y. Wu, and F. Nori, *Sc. Reports* **3**, 2943 (2013).
- [42] B. Yurke and D. Stoler, *Phys. Rev. Lett.* **57**, 13 (1986); P. Tombesi and A. Mecozzi, *J. Opt. Soc. Am. B* **4**, 1700 (1987).
- [43] A. Miranowicz, R. Tanaś, and S. Kielich, *Quantum Opt.* **2**, 253 (1990); R. Tanaś, Ts. Gantsog, A. Miranowicz, and S. Kielich, *J. Opt. Soc. Am. B* **8**, 1576 (1991).
- [44] A. Nunnenkamp, K. Borkje, and S. M. Girvin, *Phys. Rev. Lett.* **107**, 063602 (2011).
- [45] B. He, *Phys. Rev. A* **85**, 063820 (2012).
- [46] J. Q. Liao, H. K. Cheung, and C. K. Law, *Phys. Rev. A* **85**, 025803 (2012).
- [47] J. Q. Liao and F. Nori, *Phys. Rev. A* **88**, 023853 (2013).
- [48] X. W. Xu, Y. J. Li, and Y. X. Liu, *Phys. Rev. A* **87**, 025803 (2013).
- [49] A. Kronwald, M. Ludwig, and F. Marquardt, *Phys. Rev. A* **87**, 013847 (2013).
- [50] S. Gupta, K. L. Moore, K. W. Murch, and D. M. Stamper-Kurn, *Phys. Rev. Lett.* **99**, 213601 (2007).
- [51] M. Eichenfield, J. Chan, R. M. Camacho, K. J. Vahala, and O. Painter, *Nature (London)* **462**, 78 (2009).
- [52] J. D. Teufel, D. Li, M. S. Allman, K. Cicak, A. J. Sirois, J. D. Whittaker, and R. W. Simmonds, *Nature (London)* **471**, 204 (2011).
- [53] J. C. Sankey, C. Yang, B. M. Zwickl, A. M. Jayich, and J. G. E. Harris, *Nat. Phys.* **6**, 707 (2010).
- [54] X. W. Xu, H. Wang, J. Zhang, and Y. X. Liu, *Phys. Rev. A* **88**, 063819 (2013).
- [55] X. W. Xu, Y. J. Zhao, and Y. X. Liu, *Phys. Rev. A* **88**, 022325 (2013).
- [56] G. S. Agarwal and S. Huang, *Phys. Rev. A* **81**, 041803(R) (2010).
- [57] S. Weis, R. Riviere, S. Deleglise, E. Gavartin, O. Arcizet, A. Schliesser, and T. J. Kippenberg, *Science* **330**, 1520 (2010).
- [58] A. H. Safavi-Naeini, T. P. Mayer Alegre, J. Chan, M. Eichenfield, M. Winger, Q. Lin, J. T. Hill, D. E. Chang, and O. Painter, *Nature (London)* **472**, 69 (2011).
- [59] H. Xiong, L.-G. Si, A.-S. Zheng, X. Yang, and Y. Wu, *Phys. Rev. A* **86**, 013815 (2012).
- [60] H. Ian, Z. R. Gong, Y. X. Liu, C. P. Sun, and F. Nori, *Phys. Rev. A* **78**, 013824 (2008).
- [61] Y. Chang, T. Shi, Y. X. Liu, C. P. Sun, and F. Nori, *Phys. Rev. A* **83**, 063826 (2011).
- [62] H. Jing and X. Zhao, and L. F. Buchmann *Phys. Rev. A* **86**, 065801 (2012); H. Jing, D. S. Goldbaum, L. Buchmann, and P. Meystre, *Phys. Rev. A* **106**, 223601 (2011).
- [63] L. H. Sun, G. X. Li, and Z. Ficek, *Phys. Rev. A* **85**, 022327 (2012).
- [64] H. Wang, H. C. Sun, J. Zhang, and Y. X. Liu, *Sci. China-Phys. Mech. Astron.* **55**, 2264 (2012).
- [65] D. Breyer and M. Bienert, *Phys. Rev. A* **86**, 053819 (2012).
- [66] W. Z. Jia and Z. D. Wang, *Phys. Rev. A* **88**, 063821 (2013).
- [67] T. Ramos, V. Sudhir, K. Stannigel, P. Zoller, and T. J. Kippenberg, *Phys. Rev. Lett.* **110**, 193602 (2013).
- [68] H. Ian, Y. X. Liu, and F. Nori, *Phys. Rev. A* **81**, 063823 (2010).
- [69] H.C. Sun, Y. X. Liu, J. Q. You, E. Il'ichev, and F. Nori, e-print arXiv:1310.7323.
- [70] P. M. Anisimov, J. P. Dowling, and B. C. Sanders, *Phys. Rev. Lett.* **107**, 163604 (2011).
- [71] H. Yan, K.-Y. Liao, J.-F. Li, Y.-X. Du, Z.-M. Zhang, and S.-L. Zhu, *Phys. Rev. A* **87**, 055401 (2013); Y. Liu, J. Wu, D. Ding, B. Shi, and G. Guo, *New J. Phys.* **14**, 073047 (2012); G.-Q. Yang, P. Xu, J. Wang, Y. Zhu, and M. S. Zhan, *Phys. Rev. A* **82**, 045804 (2010); S. A. Moiseev and B. S. Ham, *Phys. Rev. A* **73**, 033812 (2006); J. Wang, Y. Zhu, K. J. Jiang, and M. S. Zhan, *Phys. Rev. A* **68**, 063810 (2003).
- [72] L. He, Y.X. Liu, S. Yi, C. P. Sun, and F. Nori, *Phys. Rev. A* **75**, 063818 (2007).
- [73] R. W. Boyd, *Nonlinear Optics* (Academic Press, New York, 2010).
- [74] S. Mancini and P. Tombesi, *Phys. Rev. A* **49**, 4055 (1994).
- [75] D. F. Walls and G. J. Milburn, *Quantum Optics* (Springer, Berlin, 1994).
- [76] S. Huang and G. S. Agarwal, *Phys. Rev. A* **81**, 053810 (2010).
- [77] M. Orszag, *Quantum Optics* (Springer, Berlin, 2000).
- [78] H. Wang *et al.*, in preparation (2014).